American Journal of Nano Research and Applications
2024; 12(2): 29-44
http://www.sciencepublishinggroup.com/j/nano
doi: 10.11648/j.nano.20241202.12
ISSN: 2575-3754 (Print); ISSN: 2575-3738 (Online)

Heat and Mass Transfer on MHD Nanofluid Flow with Temperature-dependent Viscosity in the Presence of Chemical Reaction

Waheed Abdelwahab Ahmed[1, 2], Edward Richard Onyango[3, *], David Theuri[3], Faiz Awad[4]

[1]Department of Mathematics, Pan African University Institute for Basic Sciences, Technology and Innovation, Juja, Kenya
[2]Department of Mathematics, Faculty of Mathematical and Computer Sciences, University of Gezira, WadMadni, Sudan
[3]Department of Pure and Applied Mathematics, Jomo Kenyatta University of Agriculture and Technology, Juja, Kenya
[4]Department of Mathematics, Omdurman Islamic University, Omdurman, Sudan

Email address:

abdelwahab.waheed@students.jkuat.ac.ke (Waheed Abdelwahab Ahmed), edward.onyango@jkuat.ac.ke (Edward Richard Onyango), dtheuri@gmail.com (David Theuri), Awad.fga@gmail.com (Faiz Awad)
[*]Corresponding author

To cite this article:

Waheed Abdelwahab Ahmed, Edward Richard Onyango, David Theuri, Faiz Awad. (2024). Heat and Mass Transfer on MHD Nanofluid Flow with Temperature-dependent Viscosity in the Presence of Chemical Reaction. *American Journal of Nano Research and Applications, 12*(2), 29-44. https://doi.org/10.11648/j.nano.20241202.12

Received: 18 November 2024; **Accepted:** 2 December 2024; **Published:** 23 December 2024

Abstract: The paper investigated the effects of heat and mass transfer with the chemical reaction on time-dependent magnetohydrodynamic (MHD) free convection nanofluid flow through a vertical plate embedded in porous media. The flow problem is expressed as a set of time-dependent dimensional nonlinear partial differential equations, which are transformed into nonlinear partial differential equations (PDEs) in dimensionless form and then solved numerically using the bivariate spectral relaxation method (BI-SRM). The effect of the significant flow parameters such as Eckert number, Joule heating parameter, magnetic parameter, thermal Grashof number, mass Grashof number, Prandtl number, chemical reaction parameter, Schmidt number, and Reynolds number on both velocity components, temperature, concentration, and induction profiles is examined. Additionally, the effects of system parameters on heat and mass transport rates and primary and secondary shear stresses are investigated and shown in tabular and graphical form. It is established that by increasing the Schmidt number or chemical reaction parameter, the Sherwood number increases, while the reverse trend is seen on the concentration distribution for increasing either Schmidt number or chemical reaction parameter. The findings of the study play a significant role in enhancing the performance and proficiency of various engineering applications, such as new-generation washing machines and engineering applications found in the fields of oil refining and biomedical engineering.

Keywords: Variable Magnetic Field, Variable Viscosity, Spectral Method, Joule Heating, Permeability, Chemical Reaction

1. Introduction

Mass transfer is constantly present in conjunction with the heat transfer process in many real-world scenarios, including chemical reactions, evaporation, condensation, and so on. The knowledge of coupled heat and mass transport can help in a number of technology transfer procedures. The literature has also extensively studied free convection flows with conjugate effects of heat and mass transfer past a vertical plate because of their engineering and industrial applications in geothermal systems, food processing, the production of polymers, and the manufacture of fibre and granular insulation. In many industrial processes, such as the synthesis of polymers and the manufacture of ceramics or glassware, challenges involving combined heat and mass transfer with chemical reactions are significant. Homogeneous and heterogeneous reactions are the two different categories of chemical reactions. While a heterogeneous reaction takes place just in a small area or at the phase boundary of the system, a homogeneous reaction happens evenly across the specified phase. Reactions in

chemical reactions can be divided into zero-order, first-order, or mixed-order reactions. Whereas the reaction rate in first-order reactions is directly proportional to the concentration itself and that in second-order reactions is proportional to the concentration of the square of a single reactant or the product of the concentrations of two reactants, the reaction rate in zero-order reactions is constant and independent of the concentration of the reactants. Choi [1] originally presented the idea of nanofluids in 1995, when he suggested dispersing solid particles smaller than a nanometer in a base liquid or fluid with poor thermal conductivity, such as water, ethylene glycol, and oils. Nanofluids have a wide range of uses, including in the treatment of cancer, smart fluid, biological science, biomedicine, industrial cooling, vehicle engines, the solar industry, nuclear reactors, and the electronics sector, among others. All of these diverse uses compelled a number of researchers [2–9] to do extensive study on heat and mass transfer in nanofluid flow in the presence of chemical reactions under various conditions.

MHD flows are of interest because they are utilised to heal wounds and cancer tumours, lessen bleeding during surgeries, deliver specific medications using magnetic particles, and diagnose illness. MHD is a topic of physics where the interaction of magnetic fields and fluid movement is investigated. The application of MHD viscous nanofluid flows in various engineering and technological fields, as well as in astronomy, geophysics, and nuclear research, has increased awareness of the issues related to temperature and mass transfer. Hamad and Pop [10] has theoretically and analytically looked into the problem of time-dependent MHD nanofluid flow through a rotating frame that contains a moving, vertical, permeable, semi-infinite flat plate with a constant heat source. Salem [11] quantitatively explored the problem of temperature-dependent viscosity, viscous dissipation, and chemical reaction impacts on steady MHD micropolar fluid flow through a long penetrable stretching sheet embedded in a non-darican porous medium using the shooting technique. Satya and Venkateswarlu [12] investigated the effects of a heat source and chemical reaction on the time-dependent MHD nanofluid natural convection flow past a semi-infinite flat plate in a rotating frame in the presence of heat and mass transfer, and closed-form analytical solutions for the governing flow equations were developed. Qureshi et al. [13] used the shooting method to numerically study the radiative heat effects on time-dependent MHD nanofluid flow in the presence of spherical Au-metallic nanoparticles after reducing the partial differential equations governing the flow using similarity transformations. Rasheed et al. [14] used the Homotopy analysis technique to investigate the effects of Joule heating and varied viscosity on two dimensional (2D) MHD Casson fluid flow across a stretched sheet. Prasadet al. [15] used the small perturbation approach in order to investigate the MHD natural convective heat and mass transfer flow of two different types of nanofluids (Cu-water and TiO2-water) bounded by a semi-infinite flat plate. MHD forced convective slip nanofluid flow across a flat plate was studied by Singh et al. [16]. The adaptive Runge-Kutta technique was used to quantitatively solve the governing nanofluid equations. Ahmmed et al. [17] has looked into the unsteady MHD natural convection nanofluid flow across an exponentially accelerated inclined porous plate under the influence of changing viscosity, thermal conductivity, and radiation. The explicit finite difference approach was used to numerically solve the coupled system of nonlinear PDEs regulating the flow. An inclined MHD Casson nanofluid flow with varying viscosity, heat, and mass diffusion across a stretched plate was investigated by Khan et al. [18]. Also, a novel model by Ahmed et al. [19] presents unsteady MHD flow in carbon nanotubes in the presence of heat transfer and variable viscosity over a shrinking porous surface is investigated. The resulting nonlinear PDEs were numerically solved using the Keller box method after it reformed to ordinary differential equations (ODEs) set via suitable transformations. Krishna et al. [20], Krishna et al. [21], and Krishna [22] discussed the effects of Hall and ion slip, both with and without consideration of nanoparticles with MHD convective rotational flow in porous media. Kebeede et al. [23] investigated the effects of magnetic field, chemical reaction, and heat radiation on 2D unsteady nanofluid flow via a penetrable stretching sheet using the homotopy analysis approach to conduct an analytical approximation. Using the finite element method, the effects of variable viscosity on time-dependent MHD nanofluid flow have been investigated by Ali et al. [24]. Also, the effects of Soret and Dufour, Joule heating, magnetic field, variable viscosity, and thermal radiation on MHD nanofluid flow have each been thought of independently, and a combination of two of them is documented in the following citations [25–28]. Additionally, a number of papers took into consideration the computational and analytical advancements in the analysis of MHD convective nanofluid flows [29–35]. In a wide range of applications, nanofluids have the potential to replace traditional fluids in heat transmission. They are expected to perform thermally better than conventional fluids due to the prevalence of scattered nanoparticles with high thermal conductivity. The nanoparticles used in the nanofluids can be made from metals, oxides, carbides, nitrides, or nonmetals, and the base fluid is often a conductivity fluid like water or ethylene glycol. Cu and Al_2O_3 are used as nanoparticles in Biswal et al. [36] consideration of Casson nanofluid flow, together with an appropriate base fluid. Hossain et al. [37] modifies a multiphase flow model to provide a better understanding of the bio-nanofluid flow regimes through a genuine bifurcated artery containing FeO nanoparticles. Khan et al. [38] used water as the base fluid and alumina nanoparticles implanted in porous medium with buoyancy force to study 2D stretched wall jet heat transfer nanofluid flow.

In accordance with this, we want to investigate Joule heating and viscous dissipation with chemical reaction on the flow of a temperature-dependent viscosity nanofluid through a vertical rotating plate embedded in a porous media in the presence of heat and mass transfer employing variable magnetic field.

2. Mathematical Formulation

Consider a time-dependent magnetohydrodynamic nartural convection nanofluid flow through a vertical plate embedded in a porous media with heat, mass, and chemical reaction. The fluid is assumed incompressible with temperature-dependent viscosity and free of electric polarization. At a fixed angular velocity, the fluid and plate rotate anticlockwise about the y^*-axis. The no-slip condition is satisfied. The electric force contribution is negligible compared with the magnetic force. The plate is along the x^*-axis and a uniform transverse magnetic field B_0 is applied to the plate, and induced magnetic fields B_x and B_z act in the x^* and z^* directions, respectively. A first-order chemical reaction is assumed to be homogeneous. Both the plate and the fluid are initially at rest, with uniform temperature T_∞^* and species concentration C_∞^*. Closer to the plate, the temperature and concentration levels are raised to T_w^* and C_w^*, respectively. Thermal conductivity, Darcy permeability and electrical conductivity are assumed constant. All physical parameters and variables are functions of y^* and t^* since the plate is infinitely long along the x^*-axis. Figure 1 depicts the flow system's physical model.

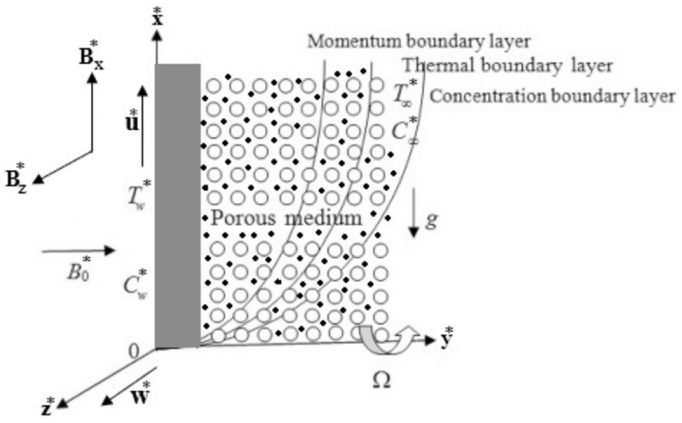

Figure 1. *Physical Model.*

The governing equations of the boundary layer flow are as follows, based on the assumptions made above:

$$\rho_{nf}\left(\frac{\partial u^*}{\partial t^*}+2\Omega w^*\right)=\frac{\mu_{nf}}{k}u^*+\frac{\partial}{\partial y^*}\left(\mu_{nf}\frac{\partial u^*}{\partial y^*}\right)+\sigma_{nf}((wB_x^*-u^*B_z^*)B_z^*-u^*B_0^{*2}) + g(\rho\beta)_{nf}(T^*-T_\infty^*)+g(\rho\beta^*)_{nf}(C^*-C_\infty^*) \tag{1}$$

$$\rho_{nf}\left(\frac{\partial w^*}{\partial t^*}-2\Omega u^*\right)=\frac{\mu_{nf}}{k}w^*+\frac{\partial}{\partial y^*}\left(\mu_{nf}\frac{\partial w^*}{\partial y^*}\right)+\sigma_{nf}((u^*B_z^*-w^*B_x^*)B_x^*-w^*B_0^{*2}) \tag{2}$$

$$\frac{\partial T^*}{\partial t^*}=\alpha_{nf}\frac{\partial^2 T^*}{\partial y^{*2}}+\frac{\mu_{nf}}{(\rho C_p)_{nf}}\left(\frac{\partial u^*}{\partial y^*}\right)^2+\frac{\mu_{nf}}{(\rho C_p)_{nf}}\left(\frac{\partial w^*}{\partial y^*}\right)^2+\frac{\sigma_{nf}}{(\rho C_p)_{nf}}\left[B_0^{*2}(w^{*2}+u^{*2})+(w^*B_x^*-u^*B_z^*)^2\right] \tag{3}$$

$$\frac{\partial C^*}{\partial t^*}=D_m\frac{\partial^2 C^*}{\partial y^{*2}}-k_r(C^*-C_\infty^*) \tag{4}$$

$$\frac{\partial B_x^*}{\partial t^*}=B_0^*\frac{\partial u^*}{\partial y^*}+\frac{1}{\sigma_{nf}}\frac{\partial^2 B_x^*}{\partial y^{*2}} \tag{5}$$

$$\frac{\partial B_z^*}{\partial t^*}=-B_0^*\frac{\partial w^*}{\partial y^*}+\frac{1}{\sigma_{nf}}\frac{\partial^2 B_z^*}{\partial y^{*2}} \tag{6}$$

The subsequent initial boundary conditions are:

$$u^*=0,w^*=0,T^*=T_\infty^*\text{for all}L\geqslant y^*\geqslant 0;t^*=0, \tag{7}$$

$$C^*=C_\infty^*,B_x^*=0,B_z^*=0\text{for all}L\geqslant y^*\geqslant 0;t^*=0, \tag{8}$$

$$u^*=u_0^*,w^*=0,B_x^*=B_0^*,B_z^*=B_0^*\text{at}y^*=0;t^*>0, \tag{9}$$

$$T^*=T_\infty^*+(T_w^*-T_\infty^*)\frac{t^*}{t_0^*};0<t^*\leqslant t_0^*;y^*=0;t^*>0, \tag{10}$$

$$T^*=T_w^*\text{when}t^*>t_0^*\text{at}y^*=0;t^*>0, \tag{11}$$

$$C^*=C_\infty^*+(C_w^*-C_\infty^*)\frac{t^*}{t_0^*};0<t^*\leq t_0^*;y^*=0;t^*>0, \tag{12}$$

$$C^*=C_w^*\text{when}t^*>t_0^*\text{at}y^*=0\text{for}t^*>0, \tag{13}$$

$$u^*\to 0,w^*\to 0,B_x\to 0\text{as}y^*\to\infty\text{for}t^*>0, \tag{14}$$

$$B_z\to 0,T^*\to T_\infty^*,C^*\to C_\infty^*\text{as}y^*\to\infty\text{for}t^*>0. \tag{15}$$

An empirical relationship for nanofluid characteristics might be considered as follows [10, 39]:

$$\rho_{nf} = (1-\phi)\rho_f + \phi\rho_s, \tag{16}$$

$$\mu_{nf} = \frac{\mu_f}{(1-\phi)^{2.5}}, \tag{17}$$

$$(\rho\beta)_{nf} = (1-\phi)(\rho\beta)_f + \phi(\rho\beta)_s, \tag{18}$$

$$\alpha_{nf} = \frac{\kappa_{nf}}{(\rho C_p)_{nf}}, \tag{19}$$

$$(\rho C_p)_{nf} = (1-\phi)(\rho C_p)_f + \phi(\rho C_p)_s, \tag{20}$$

$$\frac{\kappa_{nf}}{\kappa_f} = \frac{(\kappa_s + 2\kappa_f) - 2\phi(\kappa_f - \kappa_s)}{(\kappa_s + 2\kappa_f) + 2\phi(\kappa_f - \kappa_s)}, \tag{21}$$

$$\sigma_{nf} = \sigma_f \left[1 + \frac{3(\varepsilon - 1)\phi}{(\varepsilon + 2) - (\varepsilon - 1)\phi}\right], \tag{22}$$

The thermophysical parameters of the chosen base fluid (water) and nanoparticle material (copper) used for code validation are listed in the table 1 below.

Table 1. *Thermophysical properties.*

Properties	**Water**	**Copper (Cu)**
$C_p\,(J/kgK)$	4179	385
$\rho\,(kg/m^3)$	997.1	8933
$\kappa(\,W/mK)$	0.613	400
$\beta \times 10^{-5}(1/K)$	21	1.67
$\sigma(\Omega m)^{-1}$	0.05	5.96×10^7

Except for viscosity, which is expected to be an inverse function of temperature, all other fluid's characteristics are considered to be isotropic and constant. For liquid, the given viscosity function and the experimental results agree perfectly. The function given by Lai and Kulacki [40]:

$$\frac{1}{\mu_f} = \frac{1}{\mu_\infty}\left[1 + \gamma(T^* - T^*_\infty)\right] \tag{23}$$

We introduce dimensionless parameters as follows:

$$\begin{aligned}
B_x &= \frac{B^*_x}{B^*_0},\ B_z = \frac{B^*_z}{B^*_0},\ q_x = \frac{u^*}{u^*_0},\\
q_z &= \frac{w^*}{u^*_0},\ t = \frac{u^*_0 t^*}{L},\ y = \frac{y^*}{L},\\
\psi &= \frac{C^* - C^*_\infty}{C^*_w - C^*_\infty},\ \theta = \frac{T^* - T^*_\infty}{T^*_w - T^*_\infty},\\
R &= \frac{\Omega L}{u^*_0},\ K = \frac{\mu_f L}{k\rho_f u^*_0},\ Re = \frac{\rho_f u^*_0 L}{\mu_f},\\
Gr &= \frac{g\beta_f \nu_f (T^*_w - T^*_\infty)}{{u^*_0}^3},\\
Gm &= \frac{g\beta^* \nu_f (C^*_w - C^*_\infty)}{{u^*_0}^3},\\
M &= \frac{\sigma_f {\mu_e}^2 {B^*_0}^2 L}{\rho_f u^*_0},\ Pr = \frac{\mu_f Cp_f}{\kappa_f},\\
Ec &= \frac{{u^*_0}^2}{Cp_f \Delta T*},\ Je = \frac{\sigma_f {\mu_e}^2 {B^*}^2_0 \mu_f}{{\rho^2}_f Cp_f \Delta T^*},\\
Sc &= \frac{\mu_f}{\rho_f D_m},\ Kc = \frac{k_r \mu_f}{\rho_f {u^*_0}^2},\\
Re_m &= \sigma_f \mu_e u^*_0 L,\ \Delta T^* = T^*_w - T^*_\infty.
\end{aligned} \tag{24}$$

The governing equations (1)- (6) after applying the non-dimensional parameters become:

$$\frac{\partial q_x}{\partial t} + 2Rq_z = \frac{\mu_{nf}}{\mu_f}\frac{\rho_f}{\rho_{nf}}\left(K\frac{q_x}{(1+\gamma\Delta\theta\theta)}\right) + \frac{\mu_{nf}}{\mu_f}\frac{\rho_f}{\rho_{nf}}\left(\frac{1}{Re}\frac{\partial}{\partial y}\left(\frac{1}{(1+\gamma\Delta\theta\theta)}\frac{\partial q_x}{\partial y}\right)\right) + \frac{\beta_{nf}}{\beta_f}ReGr\theta + ReGm\psi + \frac{\sigma_{nf}}{\sigma_f}\frac{\rho_f}{\rho_{nf}}M\left((q_zB_x - q_xB_z)B_z - q_x\right), \tag{25}$$

$$\frac{\partial q_z}{\partial t} - 2Rq_x = \frac{\mu_{nf}}{\mu_f}\frac{\rho_f}{\rho_{nf}}\left(K\frac{q_z}{(1+\gamma\Delta\theta\theta)}\right) + \frac{\mu_{nf}}{\mu_f}\frac{\rho_f}{\rho_{nf}}\left(\frac{1}{Re}\frac{\partial}{\partial y}\left(\frac{1}{(1+\gamma\Delta\theta\theta)}\frac{\partial q_z}{\partial y}\right)\right) + \frac{\sigma_{nf}}{\sigma_f}\frac{\rho_f}{\rho_{nf}}M\left((q_xB_z - q_zB_x)B_x - q_z\right), \tag{26}$$

$$\frac{Cp_{nf}}{Cp_f}\frac{\rho_{nf}}{\rho_f}\frac{\partial\theta}{\partial t} = \frac{\kappa_{nf}}{\kappa_f}\left(\frac{1}{Re}\left[\frac{1}{Pr}\frac{\partial^2\theta}{\partial y^2}\right]\right) + \frac{(\rho C_p)_f}{(\rho C_p)_{nf}}\frac{Du}{Re}\frac{\partial^2\psi}{\partial\psi^2} + \frac{\mu_{nf}}{\mu_f}\left(\frac{Ec}{Re}\frac{1}{(1+\gamma\Delta\theta\theta)}\left[\left(\frac{\partial q_x}{\partial y}\right)^2 + \left(\frac{\partial q_z}{\partial y}\right)^2\right]\right) + \frac{\sigma_{nf}}{\sigma_f}\left(JeRe\left[({q_z}^2 + {q_x}^2) + (q_zB_x - q_xB_z)^2\right]\right), \tag{27}$$

$$\frac{\partial\psi}{\partial t} = \frac{1}{ScRe}\frac{\partial^2\psi}{\partial y^2} - KcRe\psi, \tag{28}$$

$$\frac{\partial B_x}{\partial t} = \frac{\partial q_x}{\partial y} + \frac{\sigma_f}{\sigma_{nf}}\frac{1}{Re_m}\frac{\partial^2 B_x}{\partial y^2}, \tag{29}$$

$$\frac{\partial B_z}{\partial t} = -\frac{\partial q_z}{\partial y} + \frac{\sigma_f}{\sigma_{nf}}\frac{1}{Re_m}\frac{\partial^2 B_z}{\partial y^2}. \tag{30}$$

The dimensionless equations listed above (25)-(30) are connected with the nondimensionalized boundary conditions listed below:

$$q_x = 0, q_z = 0, \theta = 0, \text{for all} 1 \geqslant y \geqslant 0 \text{and} t \leq 0, \tag{31}$$

$$\psi = 0, B_x = 0, B_z = 0 \text{for all} 1 \geqslant y \geqslant 0 \text{and} t \leq 0, \tag{32}$$

$$q_x = 1, q_z = 0, B_x = 1, B_z = 1 \text{at} y = 0 \text{for} t > 0, \tag{33}$$

$$\theta = t \text{when} 0 < t \leqslant 1 \text{at} y = 0 \text{for} t > 0, \tag{34}$$

$$\theta = 1 \text{when} t > 1 \text{at} y = 0 \text{for} t > 0, \tag{35}$$

$$\psi = t \text{when} 0 < t \leq 1 \text{at} y = 0 \text{for} t > 0, \tag{36}$$

$$\psi = 1 \text{when} t > 1 \text{at} y = 0 \text{for} t > 0, \tag{37}$$

$$q_x \to 0, q_z \to 0, B_x \to 0, \text{as} y \to \infty; t > 0 \tag{38}$$

$$B_z \to 0, \theta \to 0, \psi \to 0 \text{as} y \to \infty; t > 0. \tag{39}$$

The local skin friction of primary velocity is given as

$$C_{f,x} = \frac{\tau_x}{\rho_{nf}{u_0^*}^2}; \tag{40}$$

where $\tau_x = \mu_{nf}\left(\frac{\partial u^*}{\partial y^*}\right)_{y^*=0}$ is the plate shear stress of primary velocity.

The local skin friction of secondary velocity is given as

$$C_{f,z} = \frac{\tau_z}{\rho_{nf}{w_0^*}^2}; \tag{41}$$

where $\tau_z = \mu_{nf}\left(\frac{\partial w^*}{\partial y^*}\right)_{y^*=0}$ is the plate shear stress of secondary velocity.

The local Nusselt number is given as

$$Nu_L = \frac{Lq_w}{\kappa_{nf}\left(T_w^* - T_\infty^*\right)}; \tag{42}$$

where $q_w = -\kappa_{nf}\left(\frac{\partial T^*}{\partial y^*}\right)_{y=0}$ is the plate heat flux.

The local Sherwood number is given as

$$Sh_L = \frac{Lq_m}{D_m\left(C_w^* - C_\infty^*\right)}; \tag{43}$$

where $q_m = -D_m\left(\frac{\partial C^*}{\partial y^*}\right)_{y=0}$ is the plate mass flux.

Therefore, in dimensionless form, the primary skin friction, secondary skin friction, Nusselt number and Sherwood number at the plate $y = 0$, respectively are given by

$$C_{f,x} = \frac{A1}{Re}\left(\frac{\partial q_x}{\partial y}\right)_{y=0}, \tag{44}$$

$$C_{f,z} = \frac{A1}{Re}\left(\frac{\partial q_z}{\partial y}\right)_{y=0}, \tag{45}$$

$$Nu_L = -\left(\frac{\partial\theta}{\partial y}\right)_{y=0}, \tag{46}$$

$$Sh_L = -\left(\frac{\partial\psi}{\partial y}\right)_{y=0}. \tag{47}$$

where $A1 = \frac{(1-\phi)^{-2.5}}{(1-\phi)+\phi\rho_s/\rho_f}$.

3. BI-SRM

The BI-SRM is one of the spectral methods for numerically solving systems of nonlinear partial differential equations. Magagula et al. [41] was the first to suggest BI-SRM and it has been reported that the numerical method is highly accurate and converge faster than other numerical methods presented in literature for solving cases of mathematical model similar to that considered in the current research.

The following are important steps of the BI-SRM:

1. *First Step*: The nonlinear partial differential equations were linearized using relaxation approach which entails evaluating the nonlinear terms of differential equations at previous iteration level and linear term at current iteration level.
2. *Second Step*: The approximate solutions of decoupled linearized system are assumed to be bivariate Lagrange interpolating polynomials and discretization is done using spectral collocation approach.
3. *Third Step*: The resulting system of linear algebraic equations is solved iteratively using Gauss-Seidel approach.

The technique yields very accurate results across all space and time domains. The accuracy and convergence of the method are assessed using residual error analysis and solution error analysis, respectively.

4. Results and Discussion

The main focus of this current mathematical model exploration is to investigate a time-dependent MHD natural convection nanofluid flow through a vertical plate embedded in a porous medium with heat and mass transfer and chemical reaction in a rotating system. The impacts of different physical and thermophysical parameters on the flow variables, such as velocity, temperature, concentration, magnetic induction, skin friction, Nusselt number, and Sherwood number, are presented and discussed in this section. Figures 2 and 3 show the effects of the Eckert number Ec on both primary and secondary velocities. It is seen that both primary and secondary velocities are increasing as Ec is rising. A larger prediction of the Eckert number indicates a significant buoyancy force inside the fluid flow, which raises the fluid velocities; however, in circumstances of high nanoparticle concentration, the Eckert number reduces the primary fluid velocity, as seen in Figure 2. Figures 4 and 5 illustrate how the Joule heating parameter affects both primary and secondary velocities. It is seen as Je in increasing both primary and secondary velocities.The Joule heating parameter is defined as $J = EcM$, increasing Ec and M leads in an increase in the Joule heating parameter such that large values of the Eckert number and magnetic parameter aid in increasing both velocity components.

Figures 6,7,8,9,10,12, and 13 depict the impacts of $Ec, M, Pr, Je, Gr, K,$ and R on the temperature profiles, respectively. Figure 6 outlines the impact of the Eckert number on the temperature profile. It is seen that as Ec increases, the temperature profile increases. Physically, the kinetic energy of the fluid is amplified by raising Ec, which raises the fluid's temperature since Ec connects the kinetic energy in the flow and the heat enthalpy.

The effects of the magnetic parameter M on the temperature profiles in the boundary layer are shown in Figure 7. It is seen that as M increases temperature profile increases near the plate and decreases away from the plate. In general, increasing the magnetic parameter reduces the magnitude of the velocity profiles in the boundary layer, causing the temperature to rise. Figure 8 depicts the effect of the Pandtl number Pr on temperature. It is seen that as Pr increases temperature profile increases. Physically, as Pr increases, thermal boundary layer diffusivity increases. As a result, increasing the Prandtl number improves the temperature boundary layer. Figure 9 demonstrates the impact of the Joule heating parameter Je on the temperature profile. It is observed that the temperature profile increases as Je increases. Physically, the conductor warms up due to the Joule heating parameter; as a result, the fluid's temperature rises as the Joule parameter's value increases. Figures 10 and 11 illustrate that the thermal and mass Grashof numbers Gr and Gm affect the temperature profile, repetitively. The ratio of the thermal buoyancy force to the viscous force acting on a fluid is roughly represented by the thermal Grashof number Gr and the ratio of the the mass buoyancy force to the visocus force acting on a fluid is represented by mass Grashof number Gm. The boundary layer is laminar when the temperature and mass Grashof numbers are large, and vice versa. It has been demonstrated that an increase in either mass Grashof number or thermal Grashof number, or both together, this actually puts more thermal energy into the fluid molecules and loosens the intermolecular interactions within the fluid particles. Therefore, increasing the fluid velocity profile while enhancing the local heat transfer. The penetrability parameter K impact on the temperature profile is demonstrated in Figure 12. It observed that the temperature profile increases as K increases. PPhysically, this is rationalised by the fact that increasing porosity leads to reduced thermal conductivity. The effect of rotation parameter R on temperature is shown in Figure 13.It demonstrates that as R is increased, the temperature profile increases, while the same happens for the different cases of the mass volume fraction ϕ. Physically, this happens because there is an increase in heat transfer between fluid nanoparticles as a result of a higher rate of fluid constituent collisions.

Figures 14 and 15 demonstrate the effects of chemical reaction Kc and Schmidt number Sc on the concentration surfaces, respectively. It seen sa Sc increases, the concentration surfaces decreases while it is time-dependent surfaces. Physically, as Sc increases, the molecular diffusivity of a fluid decreases, resulting in enhancement of the concentration boundary layer thickness. It is seen that as Kc decreases concentration is also decreasing, this is for the same reasons mentioned above. Furthermore, it is noted that in the absence of nanoparticle impacts, these concentration profile values follow the same trend as Krishna [22].

Figures 16 and 17 show the effect of the mass Grashof number on both the axil components of the induced magnetic field. It is observed that as Gm increases, the B_x induction profile increases, while the B_z induction profile decreases. The mass buoyancy force is divided by the viscous force represented by the mass Grashof number (Gm). Therefore, as Gm increases, the viscous force decreases, resulting in an increase in the induced magnetic field correspondingly. Figures 18 and 19 show the impact of thermal Grashof number Gr in both axial components of the magnetic induction profiles.

As Gr increases, the B_x induction profile rises, while the reverse trend is seen in the B_z induction profile as Gr increases. Thermal Grashof number Gr is defined as the ratio of buoyancy to viscous force operating on the fluid. As a result, raising Gr reduces the viscous force, which causes an increase in fluid velocity, which produces a rise in the induced magnetic field. The impact of the permeability parameter K on both axial components of the induced magnetic field is seen in figures 20 and 21. It is illustrated that as K increases, the B_x induction profile increases, whereas the opposite trend is seen in the B_z induction profile as K increases. Increasing the porosity parameter physically causes an increase in fluid velocity, which contributes to an increase in Lorentz force. The Lorentz force works in the flow direction, increasing the momentum of the fluid particle and amplifying the rise in the induced magnetic field. As a result, raising the porosity parameter increases the induction profiles of the flow in the same direction, and vice versa when the flow is in the opposite direction. Figures 22 and 23 depict the effects of the Reynolds number Re on both axial components of the induced magnetic field. As Re increases, both axial components of the induction profiles decrease. The Reynolds number Re is the ratio of inertia force to viscous force. Physically, as Re increases, viscous forces decrease, which leads to rising fluid velocities, and, in turn, a reduction in the induced magnetic field occurs as a result.

The behaviour of the Nusselt number $-Nu_L$ and Sherwood number Sh_L for various values of Re, Pr, Ec, Je, Sc, and Kc are shown in tables 2 and 3, respectively. For the various situations of nanoparticle concentration shown in table 2, the Nusselt number increases as Re, Pr, Ec, and Je increase. Table 3 shows that the Sherwood number rises when Sc, Re, and Kc rise while it has similar values in the other cases of the nanoparticle volume fraction. Also, it is clearly evident that in the absence of nanoparticale, and induced magentic field the Sherwood number under the impact of Schmidt numeber Sc and chemical reaction parameter Kc has a similar pattern to those of results obtained in Krishna [22].

Figures 24, 26, 28, 30, 32, 34, 25, 27, 29, 31, 33 and 35 show the behavior of skin friction of both primary and secondary velocities as a function of surfaces for various values of Re, ϕ, Kc, Kc, Sc, and Pr. It is noted that the skin friction near the plate for both primary and secondary velocity is increasing as the mass volume fraction increases. As the Reynolds number increases, the skin friction of the primary velocity decreases near the plate. It is shown that as Kc and Sc rises, the skin friction of both velocities rises near the plate and reduces away from it. However, for secondary velocity skin friction with Kc and Sc, the opposite is true. In the case of Pr and Ec, the skin friction of both velocities is decreasing near the plate and increasing away from the plate.

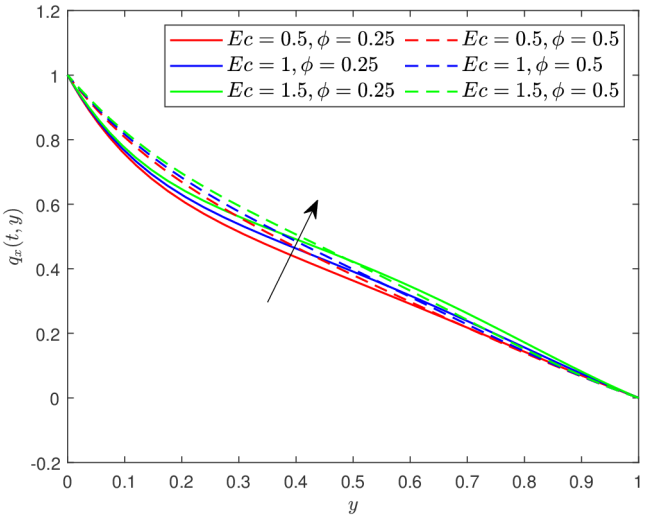

Figure 2. *Velocity $q_x(t, y)$ against Ec.*

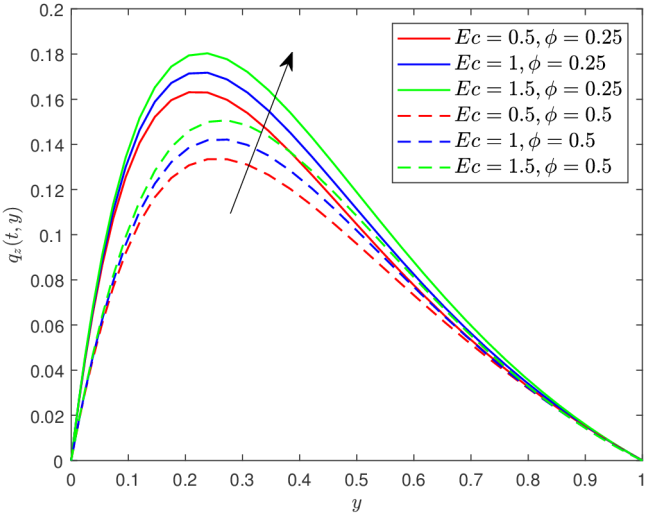

Figure 3. *Velocity $q_z(t, y)$ against Ec.*

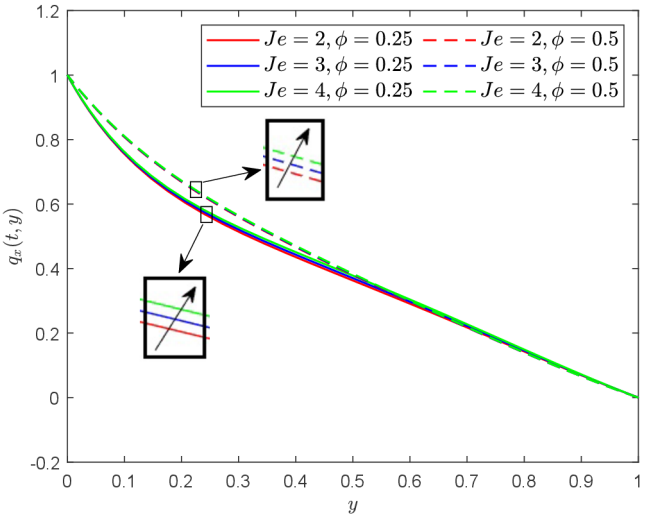

Figure 4. *Velocity $q_x(t, y)$ against Je.*

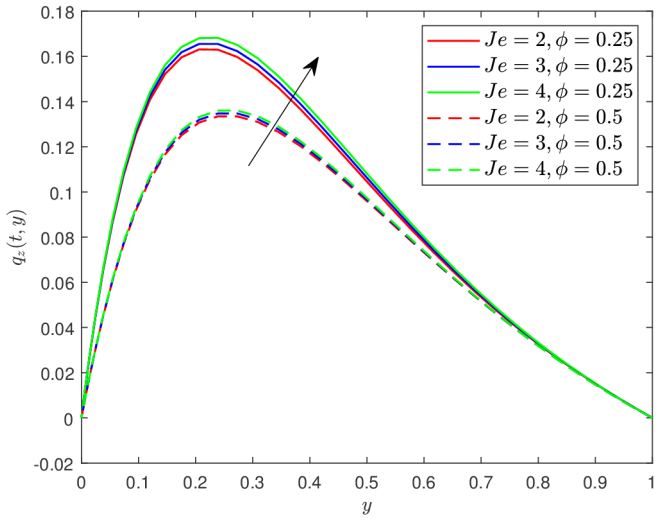

Figure 5. *Velocity $q_z(t, y)$ against Je.*

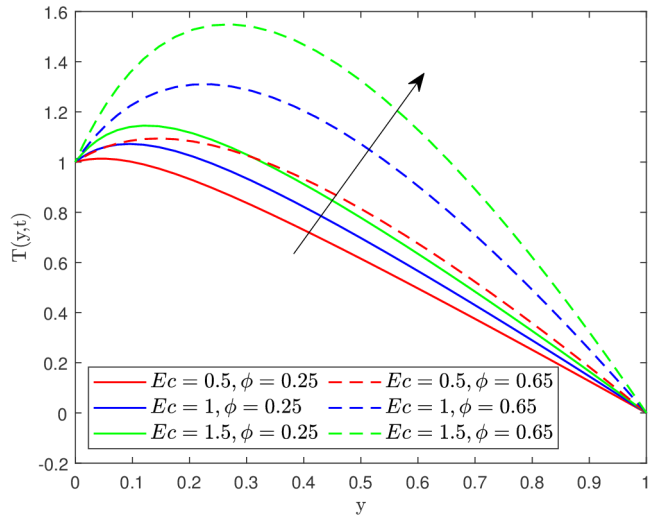

Figure 6. *Temperature $\theta(t, y)$ against Ec and ϕ.*

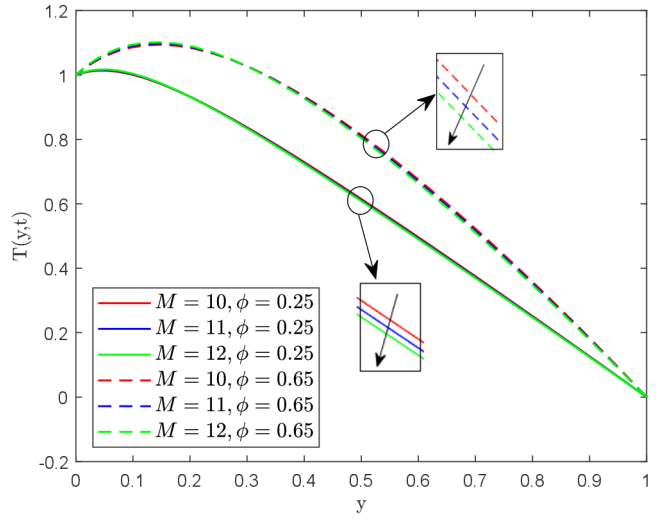

Figure 7. *Temperature $\theta(t, y)$ against M and ϕ.*

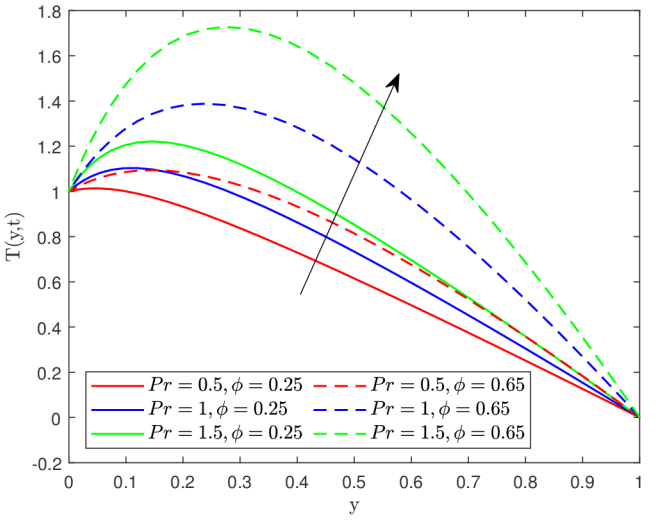

Figure 8. *Temperature $\theta(t, y)$ against Pr and ϕ.*

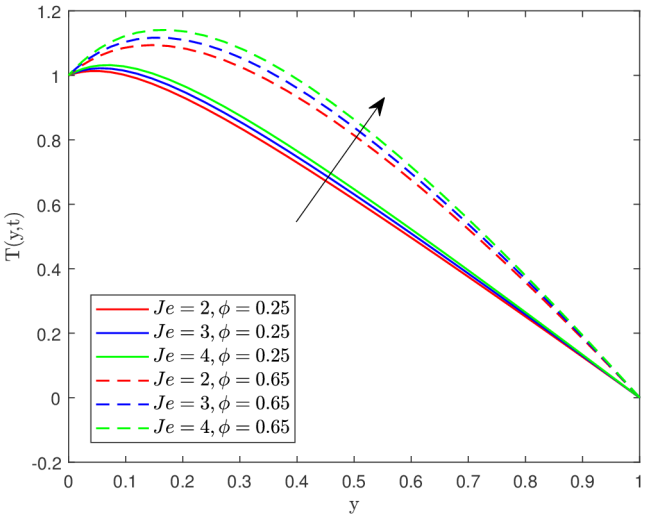

Figure 9. *Temperature $\theta(t, y)$ against Je and ϕ.*

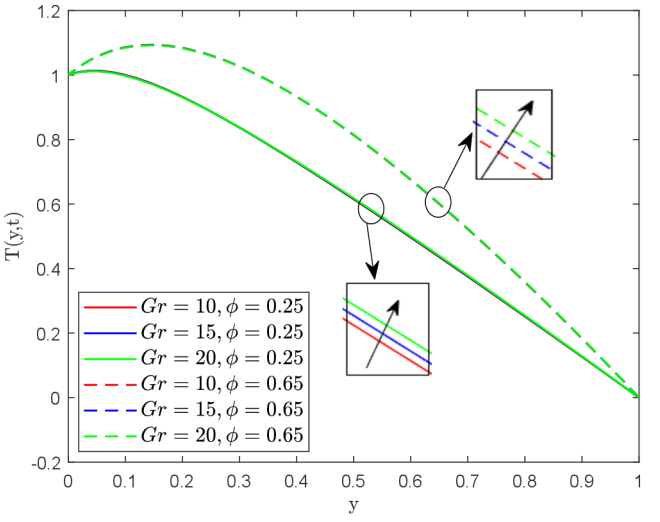

Figure 10. *Temperature $\theta(t, y)$ against Gr and ϕ.*

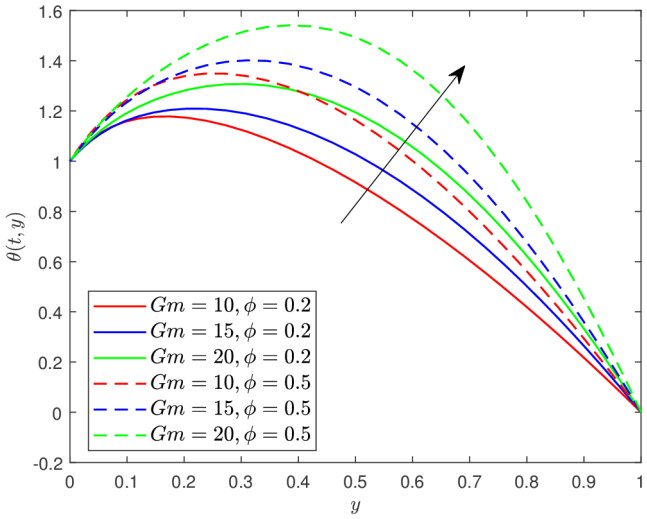

Figure 11. *Temperature $\theta(t, y)$ against Gm and ϕ.*

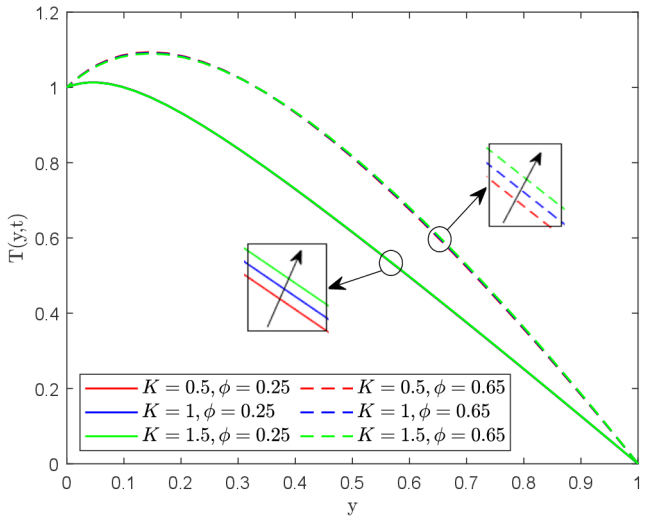

Figure 12. *Temperature $\theta(t, y)$ against K and ϕ.*

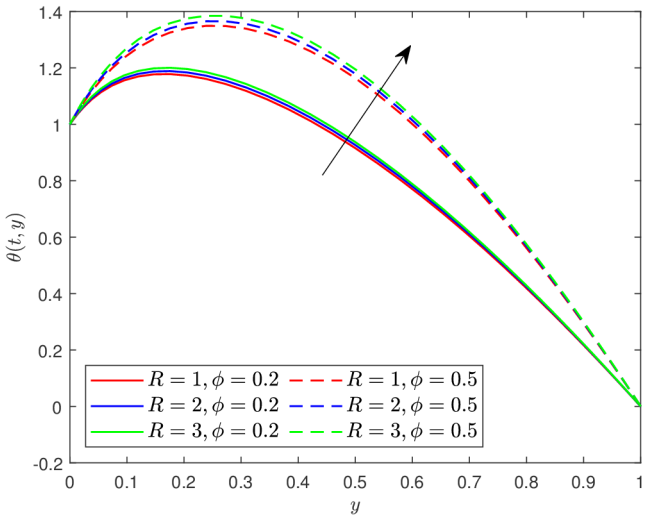

Figure 13. *Temperature $\theta(t, y)$ against R and ϕ.*

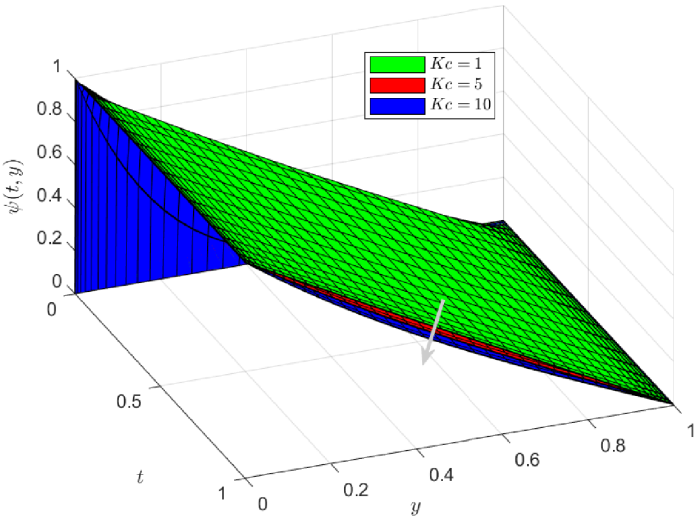

Figure 14. *Concentration $\psi(t, y)$ against Kc.*

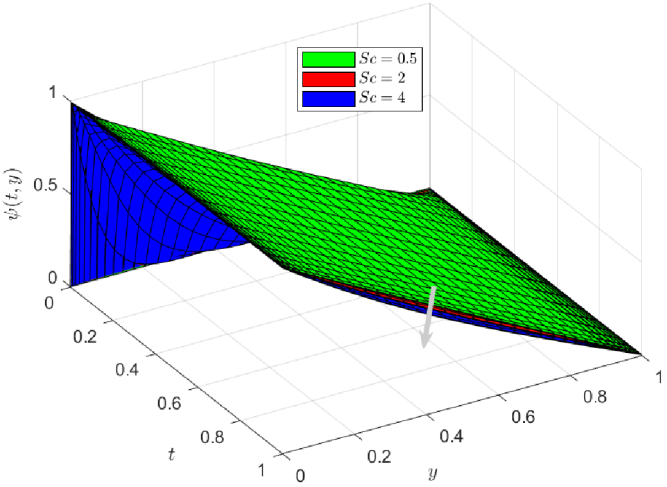

Figure 15. *Concentration $\psi(t, y)$ against Sc.*

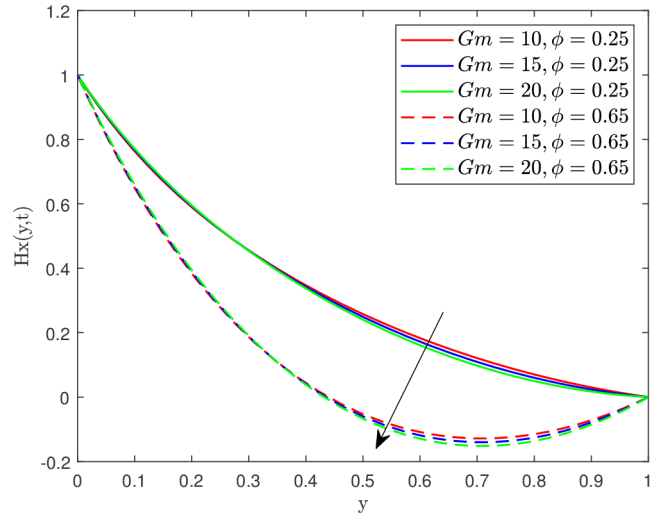

Figure 16. *Induction $B_x(t, y)$ against Gm and ϕ.*

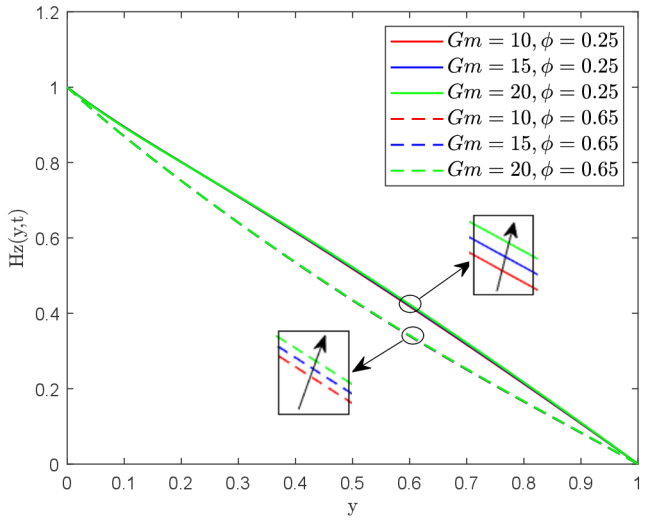

Figure 17. *Induction $B_z(t, y)$ against Gm and ϕ.*

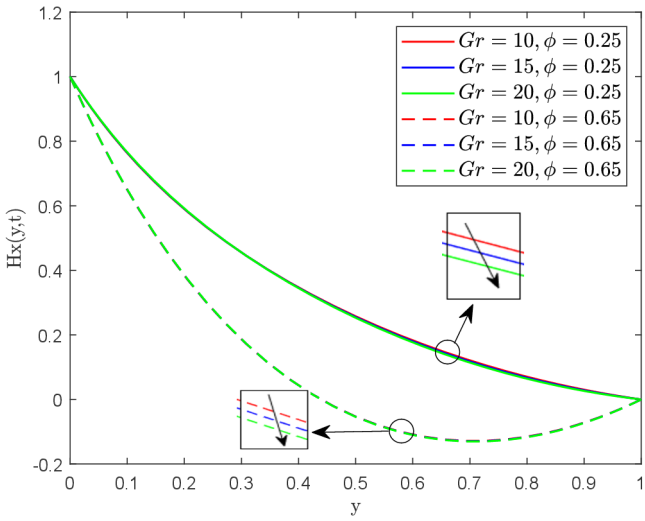

Figure 18. *Induction $B_x(t, y)$ against Gr and ϕ.*

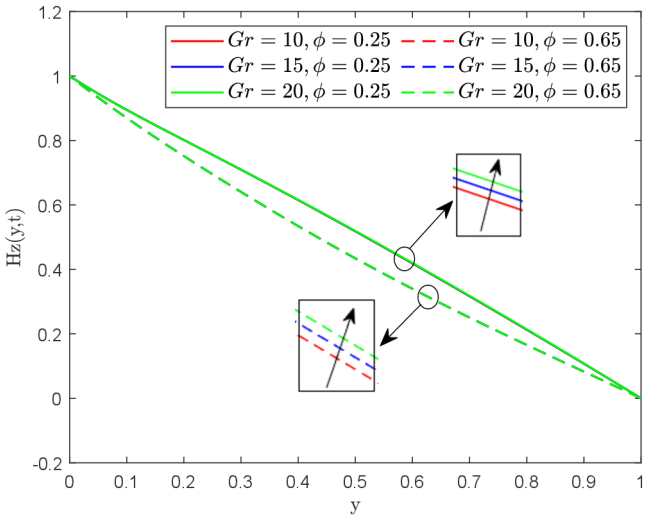

Figure 19. *Induction $B_z(t, y)$ against Gr and ϕ.*

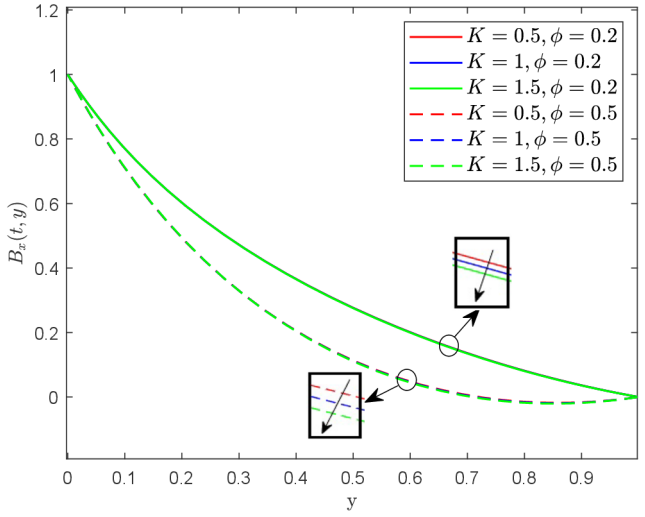

Figure 20. *Induction $B_x(t, y)$ against K and ϕ.*

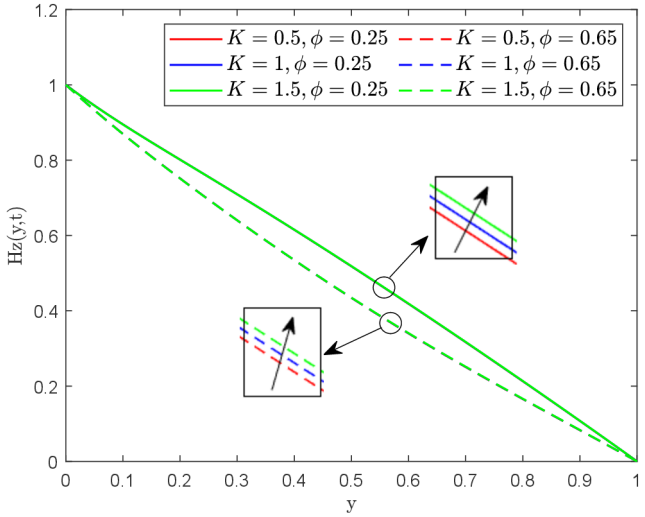

Figure 21. *Induction $B_z(t, y)$ against K and ϕ.*

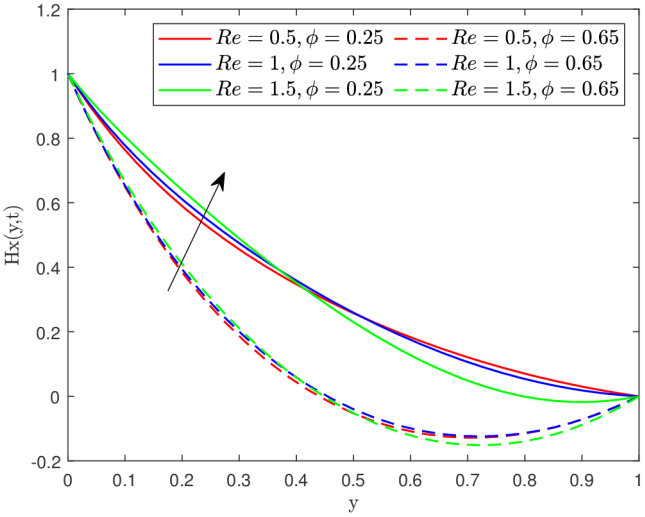

Figure 22. *Induction $B_x(t, y)$ against Re and ϕ.*

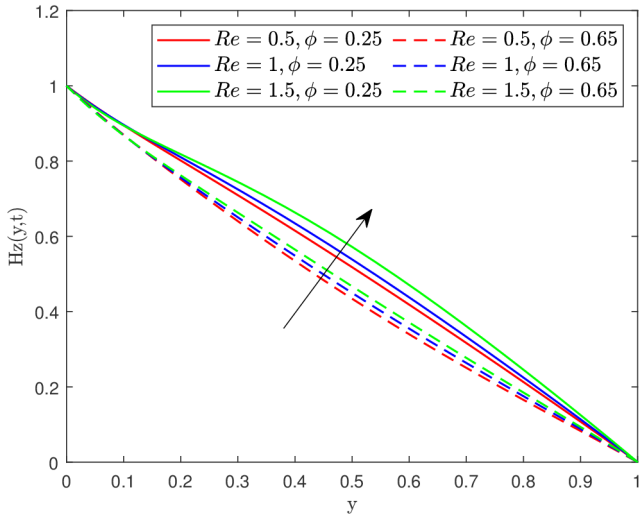

Figure 23. *Induction $B_z(t, y)$ against Re and ϕ.*

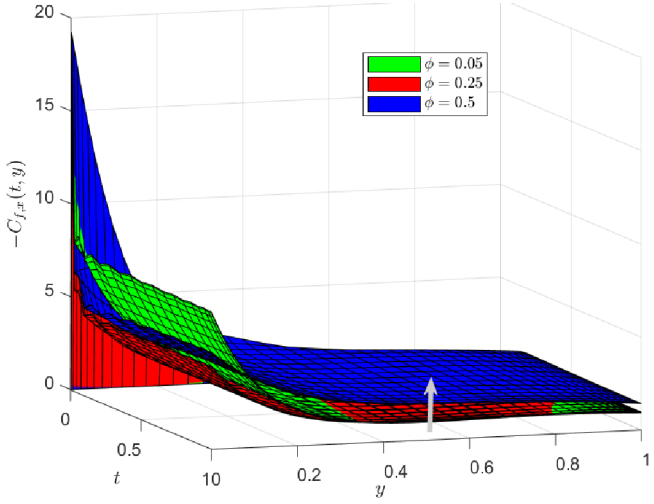

Figure 26. *The effect of ϕ on primary skin friction $C_{f,x}$.*

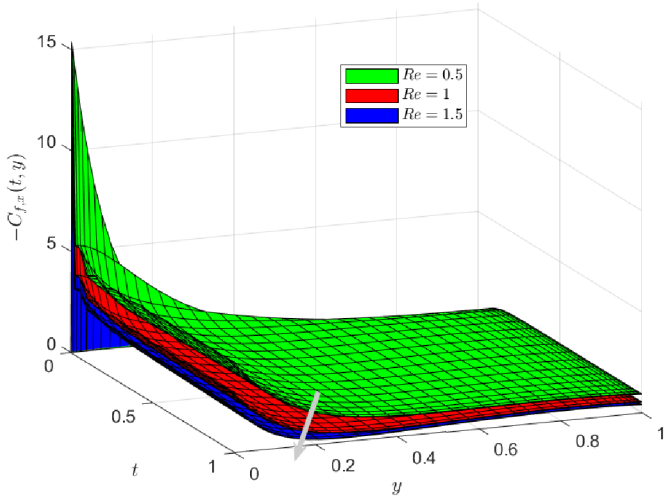

Figure 24. *The effect of Re on primary skin friction $C_{f,x}$.*

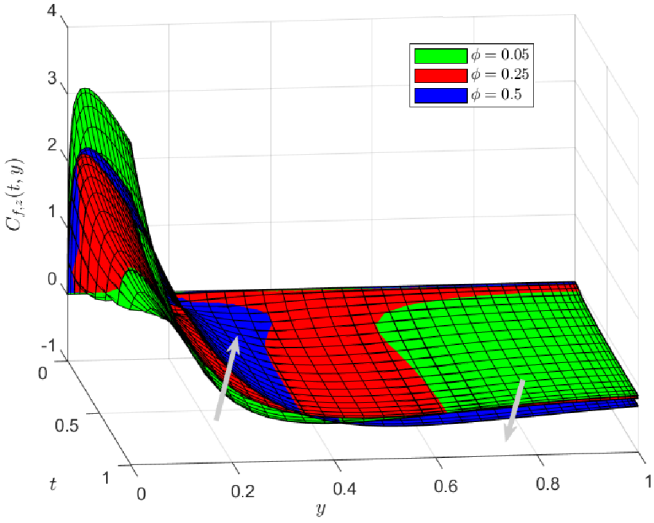

Figure 27. *The effect of ϕ on secondary skin friction $C_{f,x}$.*

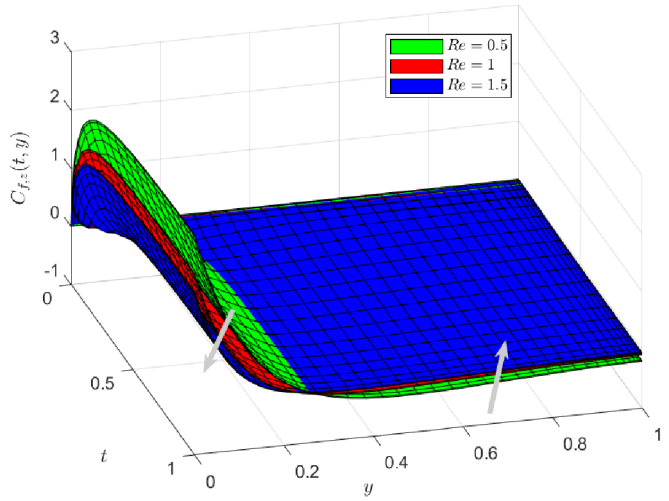

Figure 25. *The effect of Re on secondary skin friction $C_{f,z}$.*

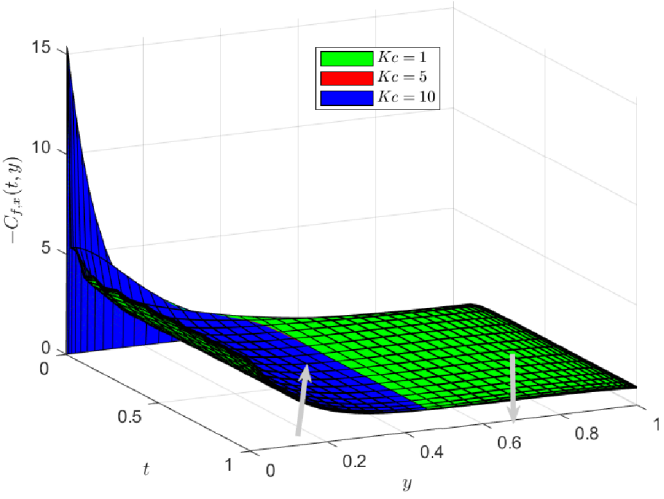

Figure 28. *The effect of Kc on primary skin friction $C_{f,x}$.*

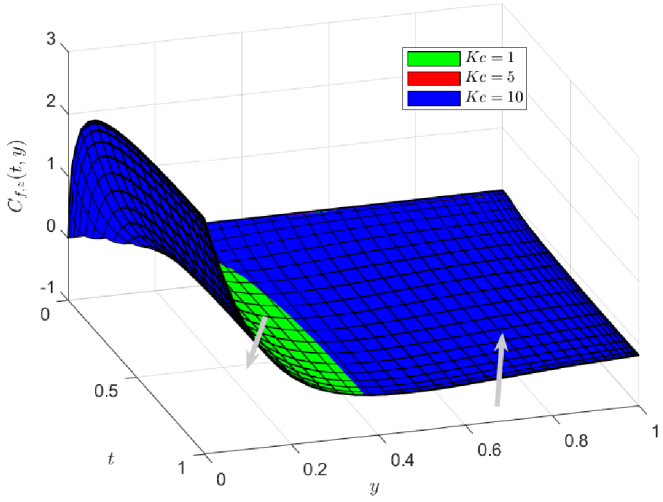

Figure 29. *The effect of Kc on secondary skin friction $C_{f,x}$.*

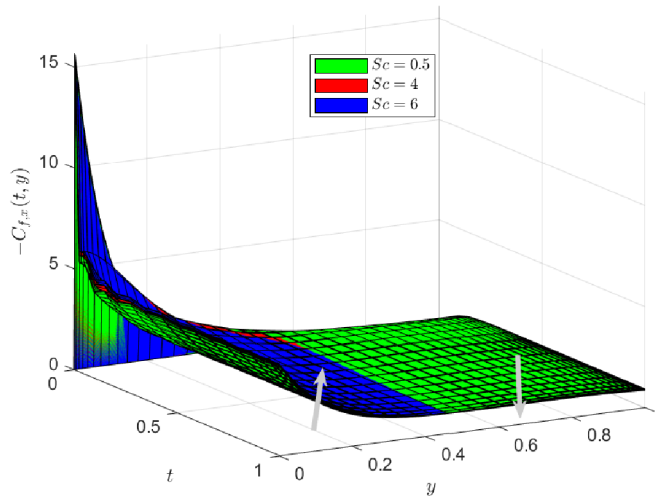

Figure 30. *The effect of Sc on primary skin friction $C_{f,x}$.*

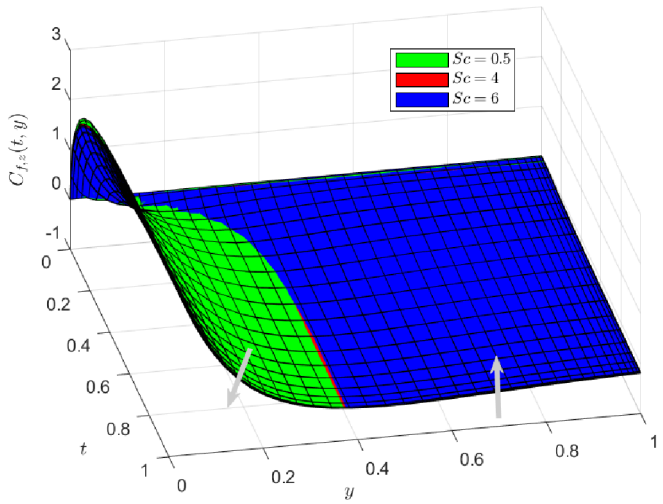

Figure 31. *The effect of Sc on secondary skin friction $C_{f,x}$.*

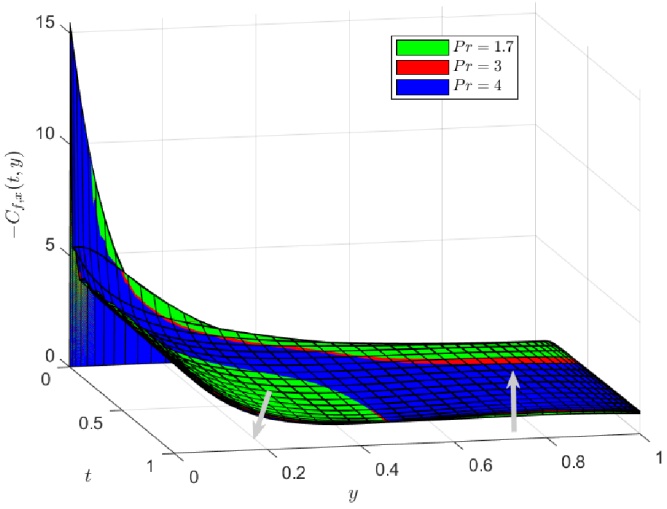

Figure 32. *The effect of Pr on primary skin friction $C_{f,x}$.*

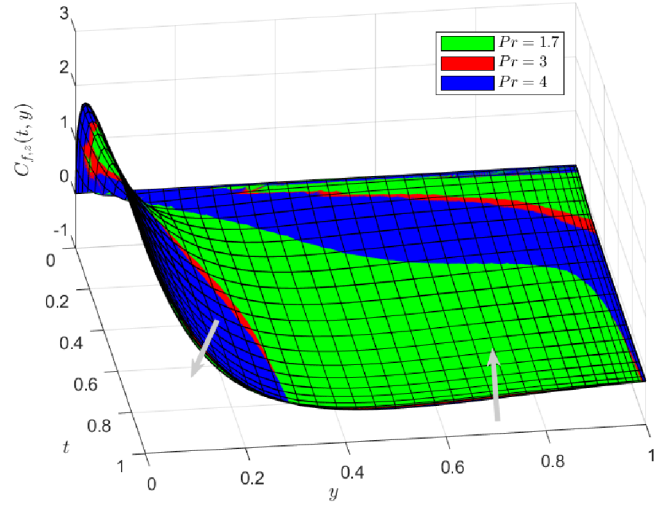

Figure 33. *The effect of Pr on secondary skin friction $C_{f,x}$.*

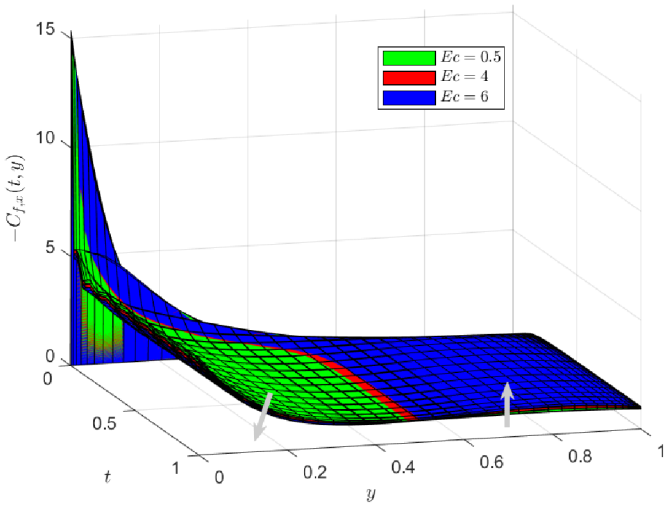

Figure 34. *The effect of Ec on primary skin friction $C_{f,x}$.*

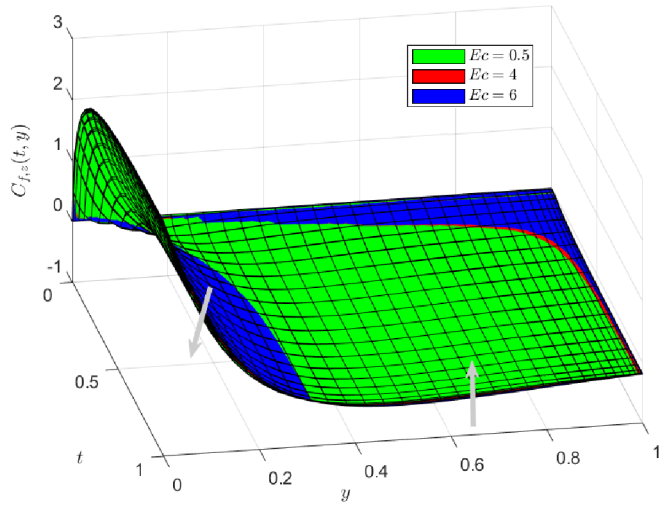

Figure 35. *The effect of Ec on secondary skin friction $C_{f,x}$.*

Table 2. *Numerical values of local Nusselt number.*

Re	Pr	Ec	Je	$-Nu_L(\phi$=0.05)	$-Nu_L(\phi$=0.2)	$-Nu_L(\phi$=0.5)
0.5	1.7	0.5	2	3.4433	2.9371	3.5614
1				7.2951	6.9889	7.5968
1.5				12.224	12.6963	13.3177
	3			6.4209	5.7314	6.9800
	4			8.4851	7.6714	9.5091
		1		6.2695	5.3631	6.5787
		1.5		8.6599	7.4539	9.2196
			3	4.0571	3.5506	4.1301
			4	4.7031	4.1881	4.7044

Table 3. *Numerical values of local Sherwood number.*

Sc	Re	Kc	$Sh_L(\phi$=0.05)	$Sh_L(\phi$=0.2)	$Sh_L(\phi$=0.5)
0.5	0.5	1	1.0332	1.0332	1.0332
1			1.0705	1.0705	1.0705
1.5			1.1079	1.1079	1.1079
	1		1.1499	1.1499	1.1499
	1.5		1.3356	1.3356	1.3356
		2	1.0739	1.0739	1.0739
		3	1.1139	1.1139	1.1139

5. Conclusions

In this exploration, we investigated the impact of heat and mass transfer on magnetohydrodynamic nanofluid flow with chemical reactions, temperature-dependent viscosity with first order chemical reaction. The BI-SRM is used to numerically solve the nonlinear partial differential equation that regulates the nanofluid flow to obtain the resulting solutions. The effects of numerous significant physical parameters on dimensionless velocity, temperature, concentration, induction, heat and mass transfer rates, and shear stresses of both primary and secondary velocities are explored, and the following results are reached:

1. Both velocity components accelerate as Ec and Je rise, while at low mass volume fraction, the primary velocity increases as Ec and Je increase.
2. An increase in $Ec, Je, Gr, Pr, K,$ and R leads to an increase in the fluid temperature, as it has been noticed that an increase in M has the opposite effect on the temperature profile of the fluid flow.
3. Increasing Kc and Sc causes the concentration profile to decrease.
4. Increasing in $Gm, Gr, K, andRe$ tends to increase the strength in the B_z magnetic induction profile, while Gr and K tend to reduce the strength in the B_x magnetic induction profile.
5. The Nusselt number rises as $Re, Pr, Ec,$ and Je increase, and the pattern is noticed for various mass volume fraction scenarios.
6. The Sherwood number rises as $Sc, Re,$ and Kc increase.

Nomenclature

u^*, w^*	x and z components of velocity, respectively(m/s)
y^*	Coordinate axis normal to the plate (m)
t^*	time (s)
B_0^*	Applied magnetic field (Wb/m^2)
B_x^*	x component of induced magnetic field (Wb/m^2)
B_z^*	z component of induced magnetic field (Wb/m^2)
T^*	temperature of nanofluid (K)
T_w^*	Wall temperature (K)
T_∞^*	temperature of the ambient nanofluid (K)
g	acceleration due to gravity (m/s^2)
C^*	Concentration (kg/m^3)
C_w^*	Wall concentration (kg/m^3)
C_∞^*	Concentration in the free stream (kg/m^3)
C_p	Specific heat (Jkg^-1K^-1)
D_m	Mass diffusivity (m^2/s)
D_1	Heat flux through concentration gradient
D_2	Mass flux through temperature gradient
k_r	Reaction coefficient
k	Permeability of the porous media(m^2)
R	Rotation parameter
K	Permeability parameter
Re	Reynolds number
Gr	Local temperature Grashof number
Gm	Local mass Grashof number
M	Magnetic field parameter
Pr	Prandtl number
Ec	Eckert number
Je	Joule heating parameter
Sc	Schmidt number
Kc	Chemical reaction parameter
Re_m	Magnetic Reynolds number
Nu_x	Local Nusselt number
Sh_x	Local Sherwood number
t_0, u_0	Initial time and initial velocity, respectively
L	Length Scale (m)
t	Dimensionless time(-)

y	Dimensionless coordinate axis normal to the plate (-)
u	Dimensionless velocity in x direction (-)
w	Dimensionless velocity in z direction (-)
B_x	Dimensionless induced magnetic field in x direction (-)
B_z	Dimensionless induced magnetic field in z direction (-)

Greek Symbols

β_{nf}	nanofluid thermal expansion coefficient (K^{-1})
μ_{nf}	nanofluid dynamic viscosity (Pa s)
ρ_{nf}	nanofluid density (kg/m^3)
β^*	Concentration expansion coefficient (K^{-1})
μ_e	magnetic permeability (H/m)
ϕ	nanoparticles volume fraction
α_{nf}	nanofluid thermal diffusivity (m^2/s)
κ_{nf}	nanofluid thermal conductivity (m^2/s)
σ_{nf}	nanofluid electrical conductivity (m^2/s)
Ω	rotation angular velocity
ψ	Dimensionless Temperature (-)
θ	Dimensionless concentration (-)

Subscripts

f	Fluid
nf	Nanofluid
s	Solid

Abbreviations

MHD	Magnetohydrodynamic
BI-SRM	Bivariate Spectral Relaxation Method
PDEs	Partial Differential Equations
ODEs	Ordinary Differential Equations
2D	Two Dimensional

ORCID

0000-0002-5315-9918 (Edward Richard Onyango)

Acknowledgments

The authors would to thank the Pan African Institute for Basic Sciences, Technology, and Innovation for providing the necessary facilities and resources to conduct this research.

Author Contributions

Waheed Abdelwahab Ahmed: Conceptualization, Formal Analysis, Investigation, Methodology, Software, Validation, Visualization, Writing - original draft, Writing - review & editing

Edward Richard Onyango: Conceptualization, Investigation, Methodology, Supervision, Visualization, Writing - review & editing

David Theuri: Conceptualization, Supervision, Visualization

Conflicts of Interest

The authors declare no conflicts of interest.

References

[1] Choi, S. US, and Jeffrey A. Eastman. Enhancing thermal conductivity of fluids with nanoparticles. No. ANL/MSD/CP-84938; CONF-951135-29. Argonne National Lab. (ANL), Argonne, IL (United States), 1995.

[2] Roy, Nepal Chandra, and Ioan Pop "Heat and mass transfer of a hybrid nanofluid flow with binary chemical reaction over a permeable shrinking surface." Chinese Journal of Physics 76 (2022): 283-298. https://doi.org/10.1016/j.cjph.2021.10.041

[3] Sudarsana Reddy, P., and P. Sreedevi. "Impact of chemical reaction and double stratification on heat and mass transfer characteristics of nanofluid flow over porous stretching sheet with thermal radiation." International Journal of Ambient Energy 43, no. 1 (2022): 1626-1636. https://doi.org/10.1080/01430750.2020.1712240

[4] Paul, Ashish, and Tusar Kanti Das. "Thermal and mass transfer aspects of MHD flow across an exponentially stretched sheet with chemical reaction." International Journal of Ambient Energy (2023): 1-12. https://doi.org/10.1002/zamm.202300935

[5] Shankar Goud, B., Dharmendar Reddy Yanala, and Abderrahim Wakif. "Numerical analysis on the heat and mass transfer MHD flow characteristics of nanofluid on an inclined spinning disk with heat absorption and chemical reaction." Heat Transfer 52, no. 5 (2023): 3615-3639. https://doi.org/10.1002/htj.22843

[6] Rehman, Aqeel ur, Zaheer Abbas, and Jafar Hasnain. "Prediction of heat and mass transfer in radiative hybrid nanofluid with chemical reaction using the least square method: A stability analysis of dual solution." Numerical Heat Transfer, Part A: Applications 83, no. 9 (2023): 958-975. https://doi.org/10.1080/10407782.2022.2156410

[7] Sedki, Ahmed M. "Effect of thermal radiation and chemical reaction on MHD mixed convective heat and mass transfer in nanofluid flow due to nonlinear stretching surface through porous medium." Results in Materials 16 (2022): 100334. https://doi.org/10.1016/j.rinma.2022.100334

[8] Arshad, Mubashar, Fahad M. Alharbi, Abdullah Alhushaybari, Sayed M. Eldin, Zubair Ahmad, and Ahmed M. Galal. "Exploration of heat and mass transfer subjected to first order chemical reaction and thermal radiation: Comparative dynamics of nano, hybrid and tri-hybrid particles over dual stretching surface." International Communications in Heat and Mass Transfer 146 (2023): 106916. https://doi.org/10.1016/j.icheatmasstransfer.2023.106916

[9] Vinodkumar Reddy, M., K. Vajravelu, P. Lakshminarayana, and G. Sucharitha. "Heat source and Joule heating effects on convective MHD stagnation point flow of Casson nanofluid through a porous medium with chemical reaction." Numerical Heat Transfer, Part B: Fundamentals (2023): 1-19. https://doi.org/10.1080/10407790.2023.2233694

[10] Hamad, M. A. A., and I. Pop. "Unsteady MHD free convection flow past a vertical permeable flat plate in a rotating frame of reference with constant heat source in a nanofluid." Heat and mass transfer 47, no. 12 (2011): 1517-1524. https://doi.org/10.1515/ijnsns-2018-0028

[11] Salem, A. M. "The effects of variable viscosity, viscous dissipation and chemical reaction on heat and mass transfer flow of MHD micropolar fluid along a permeable stretching sheet in a non-Darcian porous medium." Mathematical Problems in Engineering 2013 (2013). https://doi.org/10.1155/2013/185074

[12] Satya Narayana, P. V., and B. Venkateswarlu. "Heat and mass transfer on MHD nanofluid flow past a vertical porous plate in a rotating system." Frontiers in Heat and Mass Transfer (FHMT) 7, no. 1 (2016). https://doi.org/10.5098/hmt.7.8

[13] Qureshi, M., Qammar Rubbab, Saadia Irshad, Salman Ahmad, and M. Aqeel. "Heat and mass transfer analysis of mhd nanofluid flow with radiative heat effects in the presence of spherical au-metallic nanoparticles." Nanoscale Research Letters 11, no. 1 (2016): 1-11. https://doi.org/10.1186/s11671-016-1692-2

[14] Rasheed, Haroon Ur, Saeed Islam, Zeeshan, Tariq Abbas, and Jahangir Khan. "Analytical treatment of MHD flow and chemically reactive Casson fluid with Joule heating and variable viscosity effect." Waves in Random and Complex Media (2022): 1-17. https://doi.org/10.1080/17455030.2022.2042622

[15] Prasad, P. Durga, RVMSS Kiran Kumar, and S. V. K. Varma. "Heat and mass transfer analysis for the MHD flow of nanofluid with radiation absorption." Ain Shams Engineering Journal 9, no. 4 (2018): 801-813. https://doi.org/10.1016/j.asej.2016.04.016

[16] Singh, Padam, Alok Kumar Pandey, and Manoj Kumar. "Forced convection in MHD slip flow of alumina-water nanofluid over a flat plate." Journal of Enhanced Heat Transfer 23, no. 6 (2016). https://doi.org/10.1615/JEnhHeatTransf.2018025485

[17] Ahmmed, S. F., R. Biswas, and M. Afikuzzaman. "Unsteady magnetohydrodynamic free convection flow of nanofluid through an exponentially accelerated inclined plate embedded in a porous medium with variable thermal conductivity in the presence of radiation." Journal of Nanofluids 7, no. 5 (2018): 891-901. https://doi.org/10.1166/jon.2018.1520

[18] Khan, Mair, Amna Shahid, T. Salahuddin, M. Y. Malik, and Muhammad Mushtaq. "Heat and mass diffusions for Casson nanofluid flow over a stretching surface with variable viscosity and convective boundary conditions." Journal of the Brazilian Society of Mechanical Sciences and Engineering 40, no. 11 (2018): 1-10. https://doi.org/10.1007/s40430-018-1415-y

[19] Ahmed, Zahid, Sohail Nadeem, Salman Saleem, and Rahmat Ellahi. "Numerical study of unsteady flow and heat transfer CNT-based MHD nanofluid with variable viscosity over a permeable shrinking surface." International Journal of Numerical Methods for Heat and Fluid Flow (2019). https://doi.org/10.1108/HFF-04-2019-0346

[20] Krishna, M. Veera, and Ali J. Chamkha. "Hall and ion slip effects on MHD rotating boundary layer flow of nanofluid past an infinite vertical plate embedded in a porous medium." Results in Physics 15 (2019): 102652. https://doi.org/10.1016/j.rinp.2019.102652

[21] Krishna, M. Veera, and Ali J. Chamkha. "Hall and ion slip effects on Unsteady MHD Convective Rotating flow of Nanofluids-Application in Biomedical Engineering." Journal of the Egyptian Mathematical Society 28, no. 1 (2020): 1-15. https://doi.org/10.1016/j.aej.2020.10.013

[22] Krishna, M. Veera. "Hall and ion slip effects and chemical reaction on MHD rotating convective flow past an infinite vertical porous plate with ramped wall and uniform wall temperatures." Biomass Conversion and Biorefinery (2022): 1-18. https://doi.org/10.1007/s13399-022-03160-2

[23] Kebede, Tesfaye, Eshetu Haile, Gurju Awgichew, and Tadesse Walelign. "Heat and mass transfer in unsteady boundary layer flow of Williamson nanofluids." Journal of Applied Mathematics 2020 (2020). https://doi.org/10.1155/2020/1890972

[24] Ali, Bagh, Rizwan Ali Naqvi, Yufeng Nie, Shahid Ali Khan, Muhammad Tariq Sadiq, Ateeq Ur Rehman, and Sohaib Abdal. "Variable viscosity effects on unsteady MHD an axisymmetric nanofluid flow over a stretching surface with thermo-diffusion: Fem approach." Symmetry 12, no. 2 (2020): 234. https://doi.org/10.3390/sym12020234

[25] Das, Manik, Susmay Nandi, Bidyasagar Kumbhakar, and Gauri Shanker Seth. "Soret and Dufour effects on MHD nonlinear convective flow of tangent hyperbolic nanofluid over a bidirectional stretching sheet with multiple slips." Journal of Nanofluids 10, no. 2 (2021): 200-213. https://doi.org/10.1166/jon.2021.1784

[26] Ur Rasheed, Haroon, Abdou AL-Zubaidi, Saeed Islam, Salman Saleem, Zeeshan Khan, and Waris Khan. "Effects of Joule heating and viscous dissipation on magnetohydrodynamic boundary layer flow of Jeffrey nanofluid over a vertically stretching cylinder." Coatings 11, no. 3 (2021): 353. https://doi.org/10.3390/coatings11030353

[27] Abumandour, Ramzy, Islam M. Eldesoky, Mohamed Abumandour, Kareem Morsy, and Mohamed M. Ahmed. "Magnetic field effects on thermal nanofluid flowing through vertical stenotic artery: analytical study." Mathematics 10, no. 3 (2022): 492. https://doi.org/10.3390/math10030492

[28] Ullah, Hakeem, Mehreen Fiza, Kamal Khan, Shamaila Batool, S. M. Ghufran, and Seham M. Al-Mekhlafi. "Effect of Joule Heating and Thermal Radiation of MHD Boundary Layer Oldroyd-B Nanofluid Flow with Heat Transfer over a Porous Stretching Sheet by Finite Element Method." Journal of Nanomaterials 2022 (2022). https://doi.org/10.1155/2022/7373631

[29] Al-Farhany, Khaled, Mohammed A. Alomari, Ahmed Al-Saadi, Ali Chamkha, Hakan F. Öztop, and Wael Al-Kouz. "MHD mixed convection of a Cu-water nanofluid flow through a channel with an open trapezoidal cavity and an elliptical obstacle." Heat Transfer 51, no. 2 (2022): 1691-1710. https://doi.org/10.1002/htj.22370

[30] Prasad, K. V., C. Rajashekhar, F. Mebarek-Oudina, I. L. Animasaun, O. D. Makinde, K. Vajravelu, Hanumesh Vaidya, and D. L. Mahendra. "Unsteady Magnetohydrodynamic Convective Flow of a Nanoliquid via a Radially Stretched Riga Area via Optimal Homotopy Analysis Method." Journal of Nanofluids 11, no. 1 (2022): 84-98. https://doi.org/10.1166/jon.2022.1818

[31] Khan, Umair, Iskandar Waini, Aurang Zaib, Anuar Ishak, and Ioan Pop. "MHD mixed convection hybrid nanofluids flow over a permeable moving inclined flat plate in the presence of thermophoretic and radiative heat flux effects." Mathematics 10, no. 7 (2022): 1164. https://doi.org/10.3390/math10071164

[32] Gasmi, Hatem, Umair Khan, Aurang Zaib, Anuar Ishak, Sayed M. Eldin, and Zehba Raizah. "Analysis of mixed convection on two-phase nanofluid flow past a vertical plate in Brinkman-Extended Darcy porous medium with Nield conditions." Mathematics 10, no. 20 (2022): 3918. https://doi.org/10.3390/math10203918

[33] Abderrahmane, Aissa, Umar F. Alqsair, Kamel Guedri, Wasim Jamshed, Nor Ain AzeanyMohd Nasir, Hasan Sh Majdi, Shaghayegh Baghaei, Abed Mourad, and Riadh Marzouki. "Analysis of mixed convection of a power-law non-Newtonian nanofluid through a vented enclosure with rotating cylinder under magnetic field." Annals of Nuclear Energy 178 (2022): 109339. https://doi.org/10.1016/j.anucene.2022.109339

[34] Maneengam, Apichit, Tarek Bouzennada, Aissa Abderrahmane, Kamel Guedri, Wajaree Weera, Obai Younis, and Belgacem Bouallegue. "Numerical study of lid-driven hybrid nanofluid flow in a corrugated porous cavity in the presence of magnetic field." Nanomaterials 12, no. 14 (2022): 2390. https://doi.org/10.3390/nano12142390

[35] Eegunjobi, Adetayo Samuel, and Oluwole Daniel Makinde. "Second law analysis of MHD convection of a radiating nanofluid within the gap between two inclined concentric pipes." International Journal of Modern Physics B (2022): 2350153. https://doi.org/10.1142/S0217979223501539

[36] Biswal, Manasa Manjari, Kharabela Swain, Gouranga Charan Dash, and Swetapadma Mishra. "Study of chemically reactive and thermally radiative Casson nanofluid flow past a stretching sheet with a heat source." Heat Transfer (2023). https://doi.org/10.1002/htj.22697

[37] Hossain, SM Chapal, Mohammad Ferdows, Md Zavid Iqbal Bangalee, and Md Shariful Alam. "Two-phase bio-nanofluid flow through a bifurcated artery with magnetic field interaction." International Journal of Thermofluids 15 (2022): 100194. https://doi.org/10.1016/j.ijft.2022.100194

[38] Khan, Umair, Aurang Zaib, Anuar Ishak, Samia Elattar, Sayed M. Eldin, Zehba Raizah, Iskandar Waini, and Muhammad Waqas. "Impact of irregular heat sink/source on the wall Jet flow and heat transfer in a porous medium induced by a nanofluid with slip and buoyancy effects." Symmetry 14, no. 10 (2022): 2212. https://doi.org/10.3390/sym14102212

[39] Minea, Alina Adriana. "A review on electrical conductivity of nanoparticle-enhanced fluids." Nanomaterials 9, no. 11 (2019): 1592. https://doi.org/10.3390/nano9111592

[40] Lai, F. C., and F. A. Kulacki. "The effect of variable viscosity on convective heat transfer along a vertical surface in a saturated porous medium." International Journal of Heat and Mass Transfer 33, no. 5 (1990): 1028-1031. https://doi.org/10.1016/0017-9310(90)90084-8

[41] Magagula, Vusi M., Sandile S. Motsa, Precious Sibanda, and Phumlani G. Dlamini. "On a bivariate spectral relaxation method for unsteady magneto-hydrodynamic flow in porous media." SpringerPlus 5, no. 1 (2016): 1-15. https://doi.org/10.1186/s40064-016-2053-4